Solvent molding of organic morphologies made of supramolecular chiral polymers

Luka Đorđević,[†‡] Tomas Marangoni,[†‡] Tanja Miletić,[†] Jenifer Rubio-Magnieto,[§] John Mohanraj,[⊥] Heinz Amenitsch,[∥] Dario Pasini,[#] Nikos Liaros,[▽,○] Stelios Couris,[▽,○] Nicola Armaroli,[⊥] Mathieu Surin[§,*] and Davide Bonifazi[†,⁊,*]

[†]Department of Chemical and Pharmaceutical Sciences, INSTM UdR Trieste, University of Trieste, Piazzale Europa 1, 34127 Trieste, Italy

[§]Laboratory for Chemistry of Novel Materials, Center for Innovation in Materials and Polymers, University of Mons – UMONS, 20 Place du Parc, B-7000 Mons, Belgium

[⊥]Istituto per la Sintesi Organica e la Fotoreattività, Consiglio Nazionale delle Ricerche (CNR-ISOF), Via Gobetti 101, 40129 Bologna, Italy

[∥]Institute of Inorganic Chemistry, Graz University of Technology, Stremayrgasse 9, 8010 Graz, Austria

[#]Department of Chemistry and INSTM Research Unit, University of Pavia, Viale Taramelli 10, 27100, Pavia, Italy

[▽]Department of Physics, University of Patras, 26504 Patras, Greece

[○]Institute of Chemical Engineering Sciences (ICE-HT), Foundation for Research and Technology-Hellas (FORTH), P.O. Box 1414, Patras 26504, Greece

[⊽]Namur Research College (NARC) and Department of Chemistry, University of Namur (UNamur) Rue de Bruxelles 61, 5000 Namur, Belgium

Supporting Information Placeholder

ABSTRACT: The self-assembly and self-organization behaviour of uracil-conjugated enantiopure *(R)* or *(S)* 1,1'-binaphthyl-2,2'-diol (BINOLs) and an hydrophobic oligo(*para*-phenylene ethynylene) (OPE) chromophore exposing 2,6-di(acetylamino)pyridine termini are reported. Systematic spectroscopic (UV-Vis, CD, fluorescence, NMR and SAXS) and microscopic studies (TEM and AFM) showed that BINOL and OPE compounds undergo triple H-bonding recognition generating different organic nanostructures in solution. Depending on the solvophobic properties of the liquid media (Toluene, $CHCl_3$, $CHCl_3$/CHX and CHX/THF), spherical, rod-like, fibrous and helical morphologies were obtained, with the latter being the only nanostructures expressing chirality at the microscopic level. SAXS analysis combined with molecular modelling simulations showed that the formation of the helical superstructures is composed of dimeric double-cable tape-like structures that, in turn, are supercoiled at the microscale. This behaviour is interpreted as a consequence of an interplay between the degree of association of the H-bonded recognition, the vapour pressure of the solvent and the solvophobic/solvophilic character of the supramolecular adducts in the different solutions under static and dynamic conditions, namely during solvent evaporation conditions at room temperature.

Introduction

The control and understanding of the driving forces governing the self-assembly and self-organization[1] of functional organic molecules into complex architectures is an important research topic for developing nanostructured materials.[2] In this respect, chemists have developed several protocols to engineer functional architectures featuring programmed optoelectronic properties at different scales.[3] In particular, molecules possessing extended π-conjugated surfaces, such as oligo(phenylene ethynylene)s (OPEs),[4] oligo(phenylene vinylene)s (OPVs)[3c, 5] and coronene derivatives,[6] are versatile modules to prepare functional nanostructured materials due to their tunable electronic and optical band gap as well as their aptitude to arrange in π-π stacks. A further control in the organization can be achieved using directional non-covalent interactions, such as multiple H-bonds[3a, 3c, 3e, 7] and transition-metal coordination bonds.[8]

Whereas through molecular recognition, the preparation of architectures with controlled function and shape can be easily reached at the molecular level by inserting the right functional groups in the self-assembling molecular constituents,[9] the expression of the supramolecular structure properties at higher scales, and thus the full control of the morphological properties of microscopic structures, remains challenging.[7b, 10]

In this respect, one of the significant problems to be tackled is the establishment of protocols capable of combining the effects of chemical structures and those of the boundary conditions. From a mechanistic point of view, organic nanostructures generated by self-organization processes in solution are the result of a complex combination of several different variables. In particular, when organic materials are processed, the final morphologies are generally influenced by phenomena such as solvent dewetting and evaporation,[11] *Ostwald* ripening,[12] *Rayleigh-Bénard* instabilities,[13] *Marangoni* effect,[14] and phase separations.[15] Recently, we have shown that the geometric and spatial features of the organic morphologies generated by a supramolecular H-bonded polymer were ruled by local changes in the solution properties leading to temperature-dependent non-equilibrium diffusions of the chemical species.[16] Only a limited number of efforts have been invested to elucidate the solvent effect on the self-organization of organic morphologies.[7d, 10i, 17] This is even more important if one wanted to understand and control the transfer of molecular chirality at higher scales.[18]

We have been focusing for several years on the uracil • diamidopyridine (Ur • DAP) H-bonded complex as a heteromolecular recognition motif for preparing different hierarchically-organized materials.[19] With its moderate association constant, the Ur • DAP complex ensures a high degree of dynamicity and reversibility requisite for establishing long-range molecular order[20] in liquids[19b, 21] at liquid-solid[22] and vacuum-solid interfaces.[23] With the aim of adding an additional brick toward the understanding of the expression of molecular chirality at higher dimensions, we prepared different molecular modules (Scheme 1) and studied their self-assembly and self-organization behavior in different solvents (Chloroform ($CHCl_3$), Toluene (Tol), Chloroform/Cyclohexane ($CHCl_3$/CHX) (1:1 *v/v*) and Cyclohexane/Tetrahydrofuran (CHX/THF)) by means of complementary spectroscopic (NMR, optical and chiroptical characterization) and microscopic techniques (TM-AFM and TEM). Instead of using chiral side chains, we have employed atropoisomeric chiral cores, which consists of a *(R)*- or *(S)*-1,1'-binaphthyl-2,2'-diol (BINOL).[24] This enantiomeric couple bears two Ur moieties, while the complementary DAP units are fixed at the extremities of a chromophoric OPE spacer with lateral solubilizing alkoxy chains. Atomic Force Microscopy (AFM) and Transmission Electron Microscopy (TEM) showed a solvent-dependent formation of different organic morphologies. For instance, employing different CHX/THF solutions (80:20 – 95:5 *v/v*), nanostructures such as spheres, rods or supercoiled helices were formed, with the last being the only morphologies expressing a certain degree of macroscopic chirality. Finally, Small-Angle X-ray Scattering (SAXS) and molecular modeling simulations were used to shed further light on the molecular organization of the helical morphologies, suggesting a tape-like hierarchical organization.

Results and Discussion

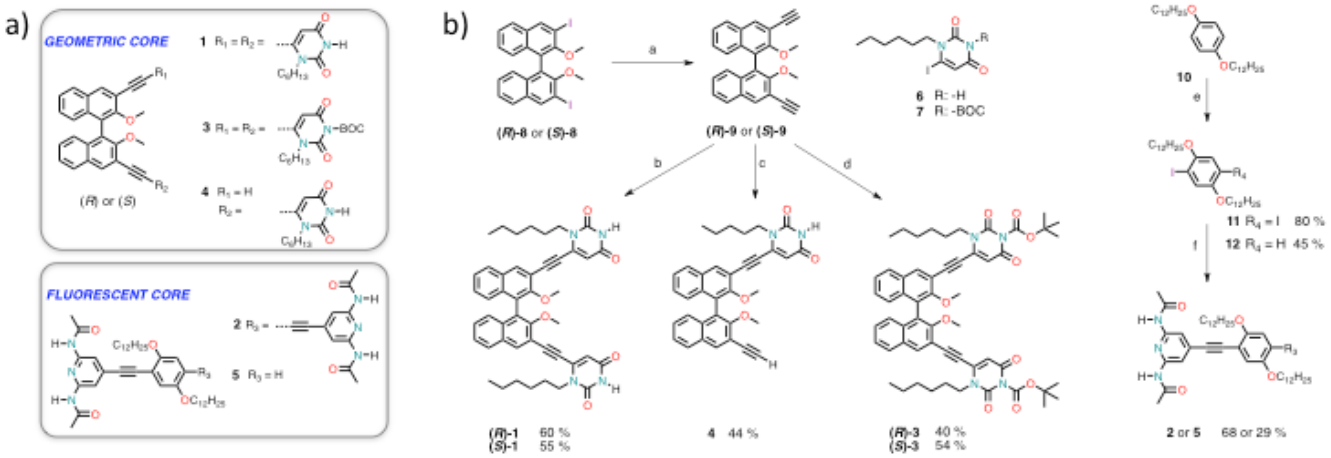

Scheme 1. (a) Molecules prepared for this study; (b) synthetic routes for molecules ***(R)*** or ***(S)*-1**, ***(R)*** or ***(S)*-3**, **2**, **4** and **5**: a) 1) TMSA, $Pd(PPh_3)_2Cl_2$, CuI, Tol/Et_3N, rt; 2) K_2CO_3, THF, MeOH; b) **6** (2.5 eq.), $Pd(PPh_3)_4$, CuI, THF/Et_3N, rt; c) **6** (0.2 eq.), $Pd(PPh_3)_4$, CuI, THF/Et_3N, rt; d) **7**, $Pd(PPh_3)_4$, CuI, THF/Et_3N, rt; e) $Hg(OAc)_2$, I_2 (2.5 or 1 eq.) , CH_2Cl_2; f) 2,6-di(acetylamino)-4-ethynylpyridine, $Pd(PPh_3)_4$, CuI, Tol/DMF/Et_3N. Abbreviations: TMSA, trimethylsilylacetylene; Tol, toluene; THF, tetrahydrofuran; DMF, dimethylformamide.

Synthesis

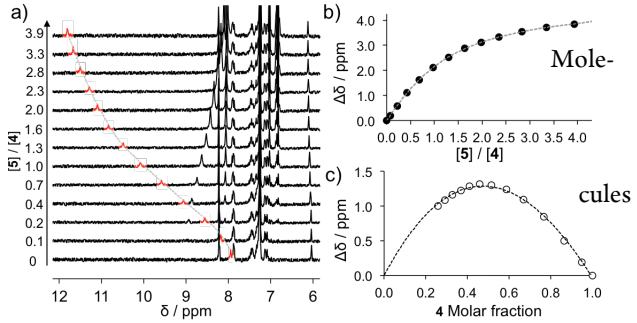

Figure 1. a) ^{1}H-NMR (400 MHz, 298 K) titration data of ***(S)*-4** in $CDCl_3$ (c = 1.3×10^{-3} M) with different molar amounts of **5** (from 0 to 3.9 equiv). N*H* peaks are highlighted in red; (b) titration data and 1:1 nonlinear least-square fitting of the N*H* signals of ***(S)*-4** plotted against the molar ratio; (c) Job's plot and fitting of the N*H* signals of ***(S)*-4** plotted against the molar fraction.

***(R)*-1** and ***(S)*-1** were synthesized by Pd-catalysed Sonogashira-Hagihara cross-coupling reaction between enantiomerically pure 3,3′-diethynyl-2,2'dimethoxy-1,1′-binaphthalenes **9**[25] and 1-hexyl-6-iodouracil **6**.[23] BOC-protected compounds ***(R)*-3** and ***(S)*-3** molecules were synthesized following an analogous pathway using N-BOC protected 1-hexyl-6-iodouracil **7**.[19b] While compound **2** was prepared according to our previously-reported procedure,[21] compound **5** results from the Pd-catalysed cross coupling of 2,6-di(acetylamino)-4-ethynylpyridine with 1,4-bis(dodecyloxy)-2-iodobenzene **12**.[21] Synthetic details are reported in Schemes 1b and S1 (SI†). The compounds were characterized by ^{1}H- and ^{13}C-NMR spectroscopies, IR, HRMS and by optical activity (Supporting Information, Fig. S1-6).

NMR investigations

The self-assembly of the complementary monotopic modules **4** and **5** was firstly studied to rationalize the influence of the lateral groups on the association behavior of the Ur • DAP recognition motif in solution (K_a, Table 1). Titration experiments in $CDCl_3$ (Fig. 1a) showed a fast equilibrium, a progressive downfield shift of the uracil N*H* protons upon the incremental addition of **5**. The association constant (Fig. 1a and 1b) was found to be 1296 (±3) M^{-1} with a 1:1 stoichiometry (as evidenced by the continuous variation method, Fig. 1c), a value which is comparable to that reported in the literature for similar systems.[20b, 22a] In apolar solvents like Tol-d_8 and $CDCl_3$/CHX-d_{12} (1:1 *v/v*), K_a values of 8737 (±627) and 14819 (±3820) M^{-1} were measured, respectively (Supporting Information, Fig. S7). As expected,[26] increasing the apolar character of the solvent mixture favored an enhancement of the binding strength. The solvent choice was also considered in case of self-complementary dimerization and was found to have only a negligible effect on the heteroassociation complexes (Supporting Information, S8-S9), as previously reported.[27] Further NMR investigations confirmed the 1:2 and 2:1 binding stoichiometry for complexes [**1**·(**5**)$_2$] and [(**4**)$_2$·**2**], respectively (Supporting Information Fig. S10). Considering the measured K_a values and assuming that the recognition motifs of the ditopic modules are independent, a mixture of complementary **1** and **2** molecules should lead to degrees of polymerization N[28] of about 0.8, 2.1 and 2.7 in $CDCl_3$, Tol-d_8 and $CDCl_3$/CHX-d_{12} (1:1 *v/v*), respectively, when working under dilute conditions (c = 2.5×10^{-4} M).

Table 1. Calculated association constants (K_a) for the H-bonded heterodimer at 298 K for **4** + **5** ⟺ [**4**·**5**], dimerization constant (K_{dim}) for **4** and the corrected association constant (K_c) **4** + **5** ⟺ [**4**·**5**] taking into account the dimerization of **4** in the reported solvents along with the solvent polarity. Calculations performed with Scientist package from MicroMath.

Solvent	ε_r	Stoichiometry	K_a, M^{-1} (sd)	K_{dim}, M^{-1} (sd)	K_c, M^{-1} (sd)
$CDCl_3$	4.81	1:1	1296 (3)	7.5 (0.1)	1300 (29)
Tol-d_8	2.44	1:1	8737 (627)	60 (5)	8205 (564)
$CDCl_3$/ CHX-d_{12}	/	1:1	14819 (3820)	19 (4)	14427 (3980)

NMR titrations in CHX/THF solutions could not be performed due to the limited solubility of both molecular components in the concentration interval needed for NMR. In order to corroborate the association of the supramolecular assemblies [**1**·**2**]$_n$, ^{1}H-NMR spectroscopy was performed on a 1:1 mixture of molecular modules ***(S)*-1** and **2** (Fig. 2a, spectra at $CDCl_3$, 500 MHz, 293 K) in $CDCl_3$. The addition of an equimolar quantity of **2** to a solution of ***(S)*-1** induced a drastic downfield of the N*H* proton resonances suggesting the formation of the *H*-bonded complex (from 8.65 to 11.10 ppm and 8.15 to 9.75 ppm for ***(S)*-1** and **2**, respectively), whereas all the other signals remained unaltered. ^{1}H-^{1}H NOESY (Fig. 2c) analysis displayed the through-space interactions between the N*H* resonances arising from the adjacent protons (N*H*-Ur and N*H*-DAP, respectively) suggesting, as expected, a close spatial proximity (< 5 Å) between the Ur and DAP moieties. The non-covalent and reversible nature of the interaction was confirmed by Variable Temperature (VT)-NMR (400 MHz, $C_2D_2Cl_4$) measurements Supporting Information, Fig. S12). Indeed, upon increasing the temperature from 293 to 373 K, a gradual reinstatement of the N*H* chemical shifts characteristic of molecules ***(S)*-1** and **2** alone were observed, clearly suggesting the gradual disruption of the *H*-bonded complex, and thus that of the supramolecular assembly (Fig. 2d). Finally, Diffusion Ordered Spectroscopy (DOSY) ($CDCl_3$, 500 MHz, Fig. 2b, Supporting Information, Fig. S11) disclosed the presence of oligomeric species, in agreement with the predicted degree of polymerization N, featuring small diffusion coefficients $D_{[1\cdot2]n}$ = 2.00

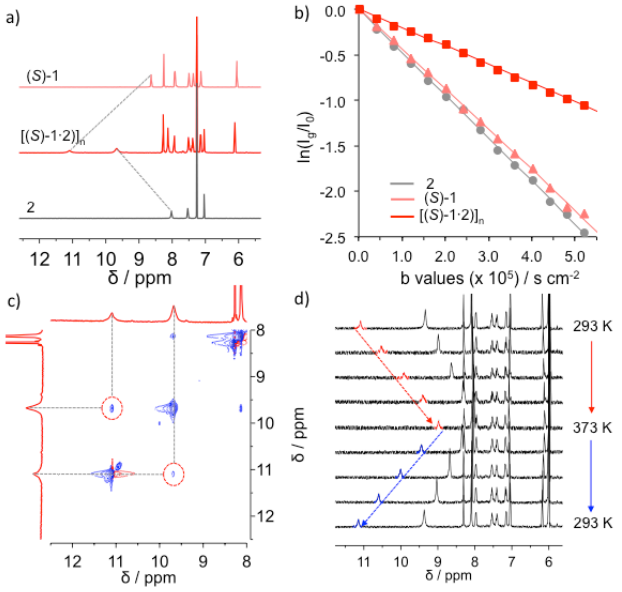

Figure 2. NMR characterization of supramolecular polymer [(*S*)-**1**·**2**]$_n$: (a) ^{1}H-NMR ($CDCl_3$, 500 MHz, 298K) of (*S*)-**1** (top), **2** (bottom) and supramolecular polymer [(*S*)-**1**·**2**]$_n$ (middle); (b) DOSY - normalized signal decay versus the diffusion weighing (b value) for (*S*)-**1** (blue), **2** (red) and supramolecular polymer [(*S*)-**1**·**2**]$_n$ (purple); (c) 2D-NOESY spectra ($CDCl_3$, 500 MHz, 298 K) of [(*S*)-**1**·**2**]$_n$; (d) VT-NMR ($C_2D_2Cl_4$, 400 MHz, 298 K) of [(*S*)-**1**·**2**]$_n$ heating and cooling cycle.

× 10^{-6} cm^2 s^{-1} (compared to D_1 = 4.37 × 10^{-6} cm^2 s^{-1} and D_2 = 4.70 × 10^{-6} cm^2 s^{-1}) owing to the formation of high-molecular-weight species, such as those deriving from the oligomeric assemblies.[29]

Molding of the morphologies

Evaporation Induced Polymerization. As mentioned in the introductory section, the evaporation of a liquid solvent plays a crucial role in the formation of various nanostructures. This effect is known as Evaporation-Induced Self-Assembly (EISA).[30] As shown for inorganic architectures, one can also expect that in supramolecular polymerization, the vapor tension of a given liquid could play a dramatic role on the degree of polymerization. In a simple model, this depends on the association strength of the recognition motif, the monomers concentration and the liquid vapor pressure at a given temperature. To evaluate these effects on our systems, we have investigated the polymerization behavior as a function of the evaporation rate of the solvent (Fig. 3, Supporting Information, Fig. S13). Thus, we have measured the normalized time-dependent shrinking of a drop-casted liquid on an AFM support plate at room temperature in an open environment under ambient pressure. Depending on the vapor pressure of the liquid, a progressive increase in the concentration of the monomers is observed, thus dynamically affecting the degree of polymerisation.[31] As outlined in Fig. 3, the higher the liquid vapor pressure (p_A), the larger the maximum degree of polymerization; for instance, at the 50 sec timepoint, the estimated N is ~15 for a solvent with higher p_A ($CHCl_3$) and ~3 for a solvent with a lower p_A (Tol). This suggests that, in evaporating $CHCl_3$ solutions, the organic morphologies are mainly controlled by the formation of longer polymers, while in Tol very shorts oligomers are preferentially formed. On the other hand, solutions with similar evaporation rates give degrees of polymerization essentially controlled by the association strength of the recognition unit. For instance, in the 1:1 *v/v* $CHCl_3$/CHX mixture higher degree of polymerization can be achieved (~40) than in $CHCl_3$ after 50 sec, this because of the stronger association of the Ur • DAP motif in apolar solutions.

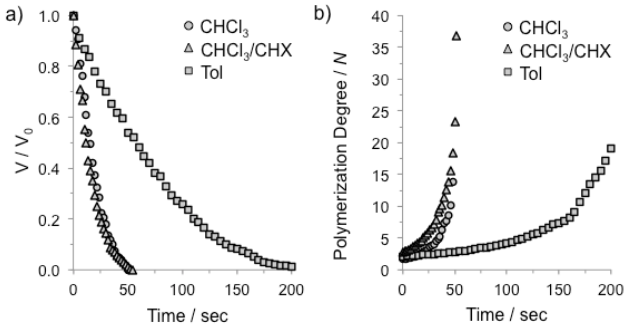

Figure 3. (a) Normalized evaporation of the solvents reported as weight lost over time and (b) estimated polymerization degree during evaporation. V and V_0 are the volume of the liquid at a t and 0 sec, respectively, calculated by measuring the weight divide by the liquid density. Vapor tension (pA) values at 20 °C and ambient pressure: 22 mmHg for Tol, 159 mmHg for $CHCl_3$ and 118 for the 1:1 *v/v* $CHCl_3$/CHX mixture (the latter value was calculated from the *Raoult's* law).

In this model, however, we did not consider the solvophobic and solvophilic properties of the solvent with respect to the monomers and the supramolecular assemblies. As previously observed for similar systems,[16] the evaporation of the solvent can also lead to concentration-driven solutal instabilities, inducing precipitation phenomena, aggregation or polymerization termination. This effect will be qualitatively considered for each solvent in the discussions of the next paragraphs.

$CHCl_3$: from solution to nanorods. Due to the chromophoric nature of the OPE spacer, UV-Vis spectra of dilute solutions were measured to gain insight into the self-assembly process. Under dilute conditions (c = 2.5 × 10^{-4} M) in $CHCl_3$, no discernible changes in the absorption profiles of [**1**·**2**]$_n$ compared to the individual compounds were noticed (Supporting Information Fig. S14), due to the weak degree of association of the Ur • DAP complex. However, when drop-casting a solution of [**1**·**2**]$_n$ (1.3 × 10^{-3} M) onto freshly cleaved mica or carbon coated grids, aggregation was observed and different nanoscopic morphologies were visualized by TM-AFM and TEM. Both techniques confirmed the presence of rod-like microstructures featuring diameters between 150 and 500 nm and lengths ranging from 0.5 to 6.5 μm. Through the combined use of both TEM and AFM phase imaging (Fig. 4, Supporting Information Fig. S27), it

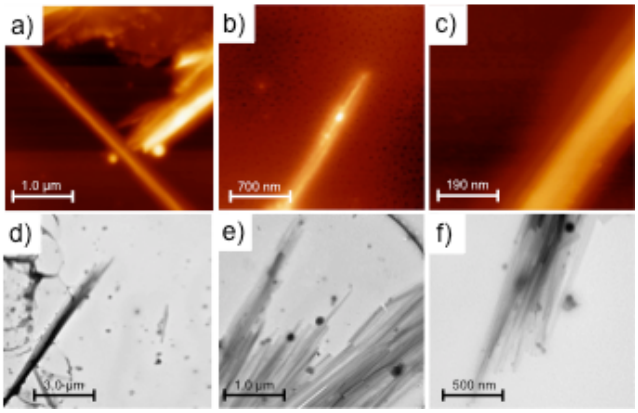

Figure 4. TM-AFM (a-c) and TEM (d-f) images of the morphologies obtained from a drop-casted $CHCl_3$ solution of $[(S)\text{-}1\cdot2]_n$ ($c = 1.3 \times 10^{-3}$ M); the other enantiomer showed the same type of nanostructuring (Supporting Information, Fig. S27).

was possible to discern rod-like structures composed of bundles of smaller fibers exhibiting a diameter of approximately 6 nm. Based on the above consideration, we can interpret these fibers as formed by short supramolecular polymers ($N \simeq 15$-20) that upon formation undergo aggregation affording the macroscopic constitutional unit of the observed morphologies. Relying on the onset condition of a concentration-driven solutal instability,[16] the extensive aggregation phenomenon seems to be governed by the solvophobic lateral alkoxy chains of compound **2**. It can be hypothesized that the $OC_{12}H_{25}$ chains are somewhat exposed on the external side of the polymeric assemblies forming a hydrophobic coat that enables extensive van der Waals interactions through chain-chain interdigitation, ultimately driving the formation of the aggregated morphologies.

Toluene: from solution to nanoparticles. Subsequently, the influence of toluene on the self-assembly was studied. The UV-Vis profile of $[\mathbf{1}\cdot\mathbf{2}]_n$ ($c = 2.5 \times 10^{-4}$ M) showed a redshift ($\lambda = 388$ nm to $\lambda = 397$ nm) of the π-π^* transition of the OPE derivative **2** and the formation of a shoulder at around 415 nm (Fig. 5a). Variable temperature measurements showed the appearance of an isosbestic point ($\lambda = 403$ nm) and an absorption profile that shifted towards the algebraic sum of the individual components (Fig. 5b, Supporting Information Fig. S18-19). Notably, the spectra were more intense at high temperatures, suggesting a scarce solubility or self-assembly of compound **2** in toluene solutions at room temperature (both scarce solubility and self-assembly of compound **2**, was confirmed by VT-UV-Vis measurments, see Supporting Information Fig. S20).[32]

Owing to the ***(R)*-1** or ***(S)*-1** intrinsic chirality and the favorable association of the Ur•DAP complex in toluene, it was possible to study the chiral assemblies by Circular Dichroism (CD) spectroscopy on both the pure components and the relative assemblies. The CD spectra ($c = 2.5 \times 10^{-4}$ M) of the BINOL derivatives were characterized by a maxi-

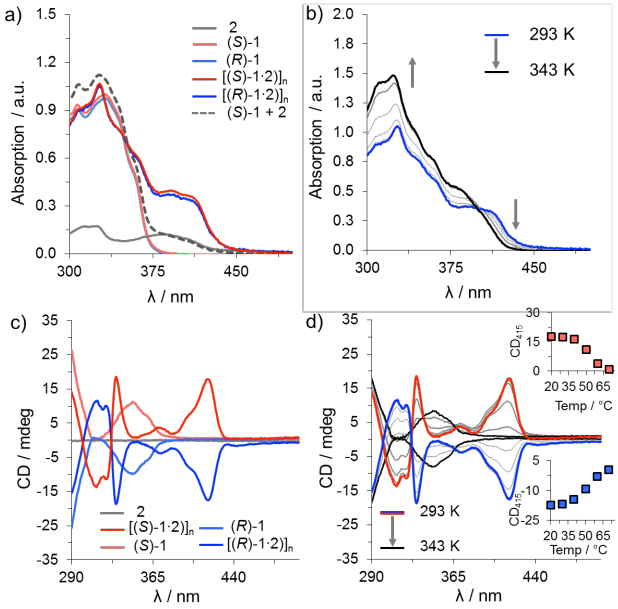

Figure 5. (a) Electronic absorption spectra of ***(S)*-1**, ***(R)*-1**, **2**, $[(S)\text{-}1\cdot2]_n$ and $[(R)\text{-}1\cdot2]_n$ in toluene at 293 K ($c = 2.5 \times 10^{-4}$ M); (b) VT absorption spectral changes in toluene from 293 to 343 K ($c = 2.5 \times 10^{-4}$ M, recorded each 5 K at a rate of 1 K/min); the same behavior was observed for the other enantiomer; (c) CD spectra of ***(S)*-1**, ***(R)*-1**, **2**, $[(S)\text{-}1\cdot2]_n$ and $[(R)\text{-}1\cdot2]_n$ in toluene at 293 K ($c = 2.5 \times 10^{-4}$ M); (d) VT-CD spectral changes of $[(S)\text{-}1\cdot2]_n$ and $[(R)\text{-}1\cdot2]_n$ in toluene from 293 to 343 K ($c = 2.5 \times 10^{-4}$ M) recorded each 10 K at a rate of 1 K/min); the inset shows the CD intensity (at $\lambda = 415$ nm) plotted versus temperature.

mum at 352 nm and an overall CD effect, which takes place in the region between 290 and 380 nm (Fig. 5c). When linear module **2** was added to a solution of ***(R)*-1** or ***(S)*-1**, a new band appeared in the region 390-435 nm with a peak around 415 nm and a shoulder around 400 nm (Fig. 5c), a spectral region in which the BINOL derivatives are not CD active. To further investigate this induced CD effect in the region where achiral **2** absorbs, the CD spectra were recorded as a function of temperature and concentration for both $[(S)\text{-}\mathbf{1}\cdot\mathbf{2}]_n$ and $[(R)\text{-}\mathbf{1}\cdot\mathbf{2}]_n$ assemblies (Fig. 5d, Supporting Information Fig. S24). VT-CD experiments from 293 to 343 K for $[\mathbf{1}\cdot\mathbf{2}]_n$ showed a gradual decrease of the induced CD effect at 415 nm, which is in accordance with the VT-UV-Vis measurements. Surprisingly, drop-casting from a toluene solution of $[\mathbf{1}\cdot\mathbf{2}]_n$ ($c = 2.5 \times 10^{-4}$ M) onto mica showed only the presence of globular, yet undefined, aggregates (Supporting Information Fig. S28). This suggests that as the solvent evaporates, the forming supramolecular assemblies undergo solutal instability already at short lengths, thus giving rise to non-structured morphologies most likely controlled by a fast matter-momentum transport in solution.

$CHCl_3$/CHX: from solution to nanofibers. The absorption profile of $[\mathbf{1}\cdot\mathbf{2}]_n$ in $CHCl_3$/CHX (1:1 *v/v*, $c = 2.5 \times 10^{-4}$ M) displayed a red-shift ($\lambda = 383$ nm to $\lambda = 390$ nm) of the π-π^* transition of compound **2** and the formation of a shoulder at $\lambda = 410$ nm (Fig. 6a). Increasing the temperature from

293 to 333 K, the absorption spectra underwent a gradual hypsochromic shift. The spectral shape at 333 K reminded that of the single components at room temperature, thus suggesting the disruption of the aggregates (Supporting Information Fig. S15). As expected, the absorption profiles were identical when performing the experiments with **(*R*)-1** or **(*S*)-1**. Additional experiments (VT-UV-Vis and CD) with reference molecules **4** and **5**, BOC-protected molecules **3**, and molecules **1** and **2** alone, did not show any significant changes in the absorption profile (Supporting Information Fig. S16, S17, S21), indicating that the spectral changes in [**1·2**]$_n$ are attributed to that on of the supramolecular assembly The same behavior was also observed by CD spectroscopy (Supporting Information Fig. S22-23).

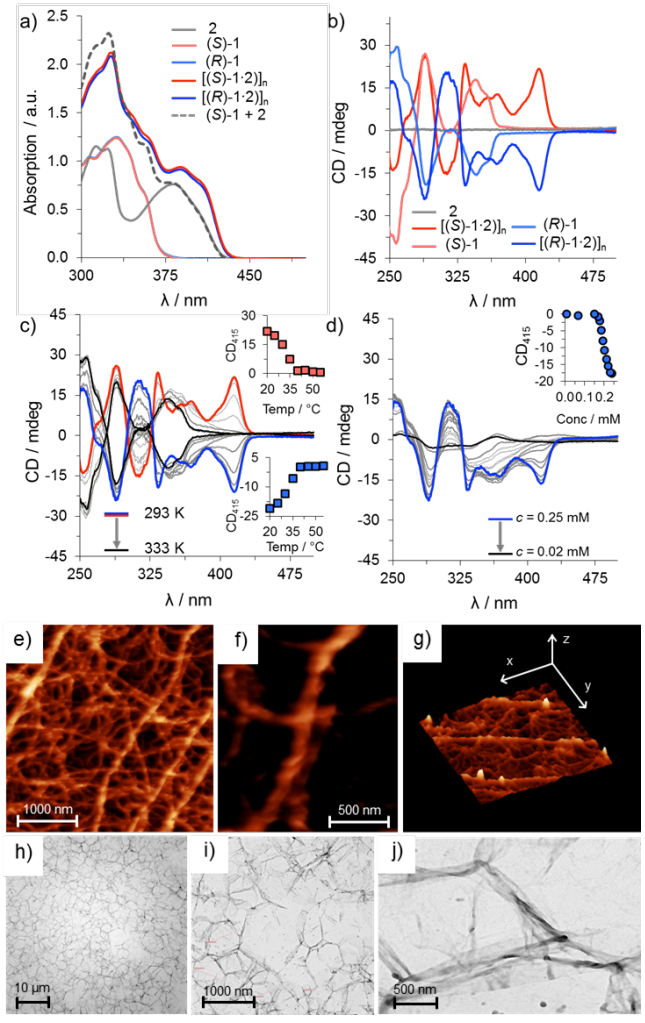

Figure 6. (a) Electronic absorption spectra of **(*S*)-1**, **(*R*)-1**, **2**, [**(*S*)-1·2**]$_n$ and [**(*R*)-1·2**]$_n$ in $CHCl_3$/CHX (1:1 *v/v*) at 293 K (c = 2.5 × 10^{-4} M); (b) CD spectra of **(*S*)-1**, **(*R*)-1**, **2**, [**(*S*)-1·2**]$_n$ and [**(*R*)-1·2**]$_n$ in $CHCl_3$/CHX (1:1 *v/v*) at 293 K (c = 2.5 × 10^{-4} M); (c) VT-CD spectral changes of [**(*S*)-1·2**]$_n$ and [**(*R*)-1·2**]$_n$ in $CHCl_3$/CHX (1:1 *v/v*) from 293 to 333 K (c = 2.5 × 10^{-4} M, recorded each 5 K at a rate of 1 K/min); insets show plot CD intensity (λ = 415 nm) versus temperature; (d) Variable concentration CD spectral changes of [**(*R*)-1·2**]$_n$ in $CHCl_3$/CHX (1:1 *v/v*) at 293 K; inset shows plot CD intensity (λ = 415 nm) versus concentration. The same behavior was also observed with the other enantiomer. TM-AFM (e-g) and TEM (h-j) images of the morphologies obtained from a drop-casted $CHCl_3$/CHX (1:1 *v/v*) solution of [**(*S*)-1·2**]$_n$ (c = 2.5 × 10^{-4} M) on mica surface and on a carbon coated grid, respectively.

In $CHCl_3$/CHX (1:1 *v/v*), the CD spectra (c = 2.5 × 10^{-4} M) of the BINOL derivatives were characterized by CD signals between 250 and 390 nm (Fig. 6b). When a linear module **2** is added to a solution of **(*R*)-1** or **(*S*)-1**, a new band appeared in the region 390-440 nm with a maximum at around 415 nm and a shoulder around 400 nm (Fig. 6b), again showing an induced CD effect in the region where achiral OPE **2** absorbs. The variation of the induced CD effect was recorded as a function of temperature and concentration for both [**(*S*)-1·2**]$_n$ and [**(*R*)-1·2**]$_n$ assemblies. As expected, both enantiomers displayed analogous spectroscopic trends (Fig. 6c). VT-CD experiments from 293 to 333 K on a solution of [**1·2**]$_n$ showed a gradual reduction of the induced CD signal at 415 nm, which is in accordance with the VT-UV-Vis measurements (Fig. S15). Similar results were also obtained when monitoring the CD profile during dilution experiments (Fig. 6d, from c = 2.5×10^{-4} M to c = 1.9×10^{-5} M). The effect of concentration on the intensity of the induced CD at 415 nm shows a sigmoidal dependence (inset of Fig. 6d), which suggests that the Ur • DAP complex governs the formation of the supramolecular architectures. Appreciably, when performing the experiments on [**(*R*)-1·2**]$_n$ and [**(*S*)-1·2**]$_n$ assemblies, the spectra were mirror images of each other (Fig. 6c).

Subsequently, the morphology of the supramolecular aggregates made of [**1·2**]$_n$ on mica surface (transferred from a $CHCl_3$/CHX (1:1 *v/v*) solution, c = 2.5 × 10^{-4} M) was studied. The TM-AFM and TEM images in Figures 6e-j showed the formation of an entangled network of fibers displaying heights ranging from 20 to 80 nm and lengths up to several µm. Although the CD spectra suggested the formation of a chiral secondary structure in a $CHCl_3$/CHX (1:1 *v/v*) solution, a microscopic helicity was not observed using AFM or TEM, even though it might be present at the nanoscopic level. This was also noticed for other supramolecular systems.[7b, 33] The formation of fibers suggested that, the higher degree of polymerization in the 1:1 *v/v* $CHCl_3$/CHX solution favors the development of fibers. Most likely, the solvophilic character of this solvent mixture disfavors aggregation phenomena and thus solutal instabilities.

CHX/THF: from solution to chiral helices. A good compromise between solubility and nanostructuration was found in a CHX/THF (95:5 *v/v*) solvent mixture. Although we could not estimate the degree of association in this solvent mixture because of the presence of precipitate at the typical concentration conditions for ^{1}H-NMR, a chiroptical profile similar to that obtained in $CHCl_3$/CHX (1:1 *v/v*) and toluene solutions was also observed for a 1:1 mixture of **1** and **2** (Fig 7d). Luminescence spectra were obtained at even more dilute concentrations (c = 3.5 × 10^{-6} M). Both molecules exhibited strong fluorescence, with related quantum yields (Φ_{fl}) of 0.12 and ≃ 1.0 for **1** and **2**, respectively. The absorption and emission features of OPE derivative **2** alone in the CHX/THF (95:5 *v/v*) mixture were red-shifted compared to more polar solvents such as MeOH and THF,[19b, 22b] indicating a strong solvophobic-driven self-aggregation of **2**, most likely through J-type association.[34] Moreover, the emission of [(*R*)-**1**·**2**]$_n$ showed a weak shoulder at longer wavelengths and, compared to a solution containing only **2**, a lower quantum yield (Φ_{fl} = 0.18) and a higher full width at half maximum (FWHM), i.e. 80 nm (**2**: 62 nm, Fig. 7c). The slight changes observed in the absorption and emission spectra of [(*R*)-**1**·**2**]$_n$ along with the lifetime values (3.4 ns for (*R*)-**1**; τ_1 = 1.5 ns; τ_2 = 3.7 ns for **2**; τ_1 = 1.2 ns; τ_2 = 4.2 ns for [(*R*)-**1**·**2**]$_n$) were ascribed to the presence of H-bonded self-organized structures in CHX/THF (95:5 *v/v*) (Fig. 7a-c, Supporting Information Fig. S26c). Notably, the emission at high temperature showed a blue shifted maximum with substantially reduced FWHM (52 nm) and the disappearance of the extended shoulder at longer wavelengths (Fig. 7c). This indicated the presence of isolated units of molecule **2** in the sample, which also exhibited much higher intensity. Owing to the high quantum yield of the monomer unit **2** (Φ_{fl} ≃ 1.0), its emission peak masked the signal from weakly emissive molecular species (i.e., (*R*)-**1**, Φ_{fl} = 0.12). In order to corroborate the presence of H-bonds between molecular species (*R*)-**1** and **2**, a H-bond disrupting polar solvent such as DMSO was added (5% *v/v*) to a solution of [(*R*)-**1**·**2**]$_n$ (Supporting Information Fig. S26a-b). Upon addition of DMSO, the absorption spectrum of [(*R*)-**1**·**2**]$_n$ shows the appearance of blue shifted bands with discernible signatures of the individual molecular units, (*R*)-**1** and **2** (Supporting Information Fig. S26). The disruption of the assembly by DMSO was also observed with the VT-fluorescence experiments. Microscopic analysis of the deposition of CHX/THF (95:5 *v/v*) solutions containing [(*R*)-**1**·**2**]$_n$, also displayed the formation of fiber-like morphologies (Fig. 7e). The fibrous structures displayed small diameters ranging from 5 to 10 nm and average lengths between 0.8 μm to 3 μm. The same morphologies were also obtained upon deposition of the chiral supramolecular systems [(*S*)-**1**·**2**]$_n$. Additional experiments revealed the formation of nanofibers that lacked apparent chirality by AFM investigation of racemic [**1**·**2**], giving further importance to the intrinsic chirality of the BINOL core (Fig. S29). As previously mentioned, CD investigations of dilute solutions containing [(*R*)-**1**·**2**]$_n$ and [(*S*)-**1**·**2**]$_n$ under the same experimental conditions showed the formation of a new band, centered at around 420 nm but presenting opposite signs (Fig. 7d). This observation, together with the formation of fibrous morphologies, can be considered as a clear proof of the transfer of chirality from the molecular scale to nanostructured nano-objects, in which the different single polymeric structures are held together by the combination of non-covalent interactions. Similarly to the case of the $CHCl_3$/CHX (1:1 *v/v*) solution, the formation of narrow fibers from CHX/THF (95:5 *v/v*) suggested that under these conditions higher degree of polymerization are achieved and no extensive aggregation is ob-

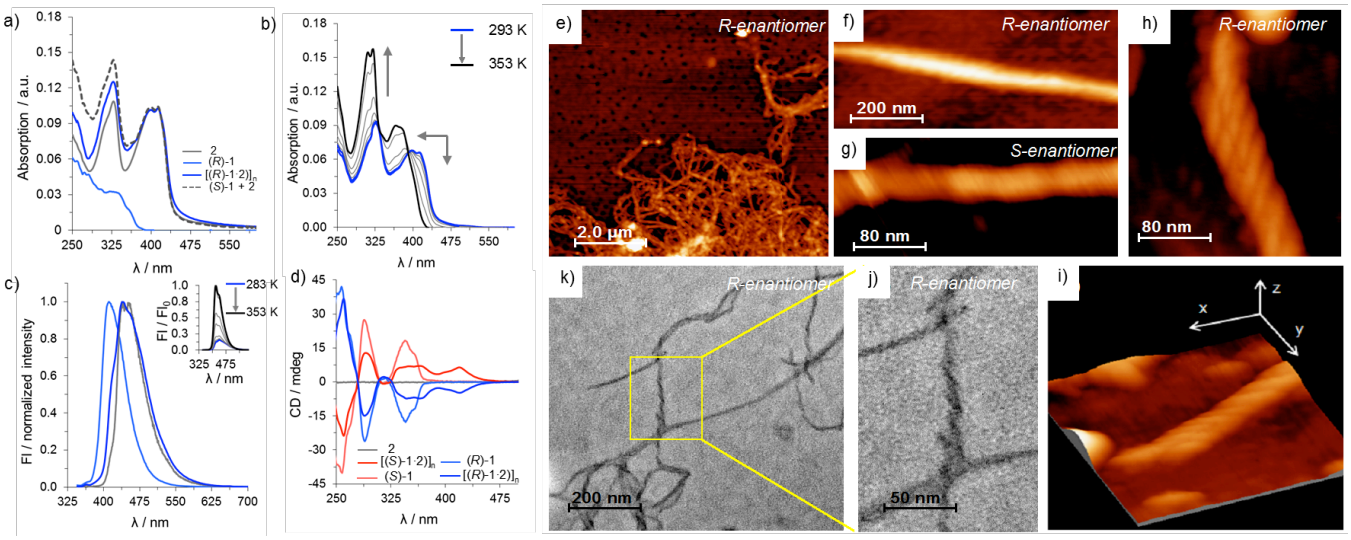

Figure 7. (a) Electronic absorption of (*R*)-**1** (light blue), **2** (grey), [(*R*)-**1**·**2**]$_n$ (blue) and algebraic sum of (*R*)-**1** and **2** (dash grey) in CHX/THF (95:5 *v/v*), c = 3.5 × 10^{-6} M; (b) Absorption spectral changes of 1:1 (c = 3.5 × 10^{-6} M) mixture of [(*R*)-**1**·**2**]$_n$ during VT measurement; (c) Normalized fluorescence spectra of (*R*)-**1** (light blue), **2** (grey), [(*R*)-**1**·**2**]$_n$ (blue) and (inset) VT-emission spectral changes of [(*R*)-**1**·**2**]$_n$ recorded each 10 K, at a rate of 1 K/min; d) CD spectra of (*S*)-**1**, (*R*)-**1**, **2**, [(*S*)-**1**·**2**]$_n$ and [(*R*)-**1**·**2**]$_n$ in CHX/THF (95:5 *v/v*) at 293 K (c = 3.5 × 10^{-6} M).TM-AFM (e-i) and TEM (k,j) images of nanofibers as obtained from drop casting a CHX/THF (95:5 *v/v*) solution of [(*R*)-**1**·**2**]$_n$ on mica surface and on a carbon coated grid, respectively (c = 1.7 × 10^{-3} M).

served. This is probably caused by the solvophilic character of these supramolecular polymers in this solvent mixture.

Nanostructuration of the chiral helices. Additional evidences for the formation of the fibrous aggregates in solution were obtained from SAXS, a powerful technique to determine the shape and size of colloidal, diluted, and particulate systems.[35] The SAXS pattern of a solution of [(*R*)-**1**·**2**]$_n$ in CHX-THF (95:5 *v/v*, $c = 1.7 \times 10^{-6}$ M) is reported in Figure 8. In order to reconstruct the three-dimensional structure adopted by the supramolecular polymer, the data have been fitted by assuming homogeneous monodisperse structural models, such as cylinders, hollow cylinders and helical bundles. The best fitting result (Fig. 8a, red line) were obtained using helical superstructure models[36] resulting from the topological twisting (angle of 36°) of a 1D nanostructure featuring a ribbon-like structure (width of 8 nm). Their structural and geometrical features of which are depicted in Figure 8b.[37]

In order to gain insight into the molecular organization of the nanofibers, molecular modeling simulations were also carried out at the atomistic level using Molecular Mechanics (MM). MM studies were performed using the COMPASS force field, which accurately describes the geometry and torsion potentials of phenylene ethynylene oligomers, alkyl groups, BINOL, and is appropriately optimized for modeling organic condensed phase and H-bonded structures.[38] Figure 9 shows the structures of the studied compounds and the molecular modeling of the *H*-bonded bi-component supramolecular networks. Conformers of (*R*)-**1** and (*S*)-**1** possess a torsional angle between the naphthalenes planes of around 96° for the t*ransoid* conformer (see Fig. 9a for the *transoid* conformation, where the 2,2'-methoxy groups are pointing in opposite directions) and 72° for the *cisoid* conformers. For linear module **2**, the *para*-phenylene ethynylene moiety has a flat torsion potential between the phenylenes (0.5 kcal/mol barrier), which dictate through the torsional angle of the BINOL units the geometrical properties of supramolecular polymers [(*R*)-**1**·**2**]$_n$ and [(*S*)-**1**·**2**]$_n$. Depending on whether one naphthyl substituent of the (*R*)-**1** or (*S*)-**1** module is facing the neighbouring naphthyl at each side of the linear linker (see sketch in Fig. 9b where equivalent naphthalenes are depicted with the same black tonality), the complementary *H*-bonding arrangement yields two possible types of bi-component networks, namely helix or zig-zag patterns (Fig. 9b). Based on a series of modeled assemblies obtained by different cycles of MM simulations, we found that square-shaped networks are indeed forming a helical assembly at the supramolecular level with a pitch made of tetrameric units of [(*R*)-**1**·**2**]$_n$ (Fig. 9c). In contrast, the zig-zag arrangement yields the formation of one-dimensional polymer, because in this setting two equivalent naphthyl substituents face each

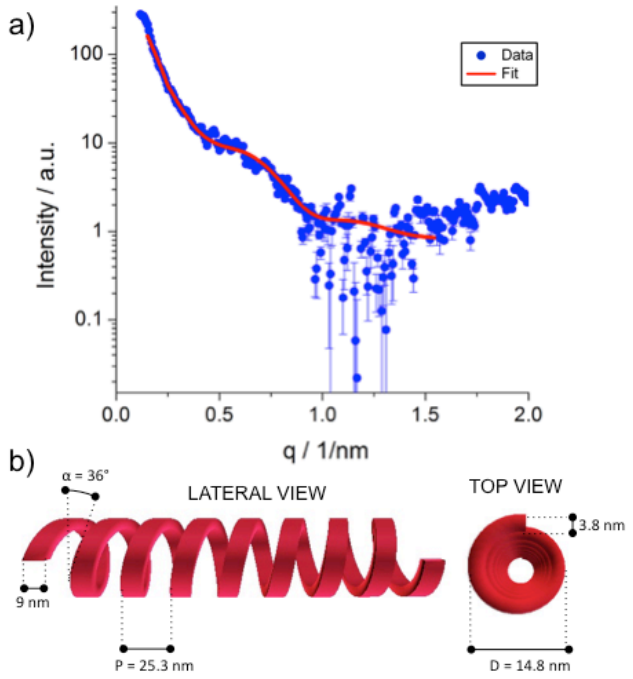

Figure 8. (a) Experimental SAXS data (blue) obtained from a solution of [(*R*)-**1**·**2**]$_n$ in CHX/THF (95:5 *v/v*) (298 K, $c = 1.7 \times 10^{-6}$ M) superimposed with a fitting model (red line) of a helical tape; (b) schematic representation of the supramolecular helicoidal fibers as obtained from [(*R*)-**1**·**2**]$_n$.

other at each termini of the linear unit (Fig. 9b). Although this type of supramolecular organization would leave large voids in the arrangement, the presence of the C_{12} alkyl groups stabilizes the formation of supercoiled double helical cables (Fig. 9c) by lateral alkyl-alkyl interdigitation. In the geometry-optimised model of [(*R*)-**1**·**2**]$_n$ shown in Figure 9c, both molecular geometries and length of the alkyl groups govern the formation of compact double helicoidal arrangement, with a single-helix pitch of around 3.8 nm (i.e. 1.9 nm from helix blue to helix yellow in Fig. 9c). The geometry of the double helix has a rectangular cross section, with a minimum distance of around 2.8 nm from side to side and a maximum distance of around 5.0 nm from corner to corner. Indeed, such compact packing is very likely more stable than the zig-zag arrangement in apolar solvents, as the alkyl groups point at the outer surface of the helix. Notably, the geometrical parameters obtained from the MM simulation are in strict relationship with the structural data obtained from the SAXS analysis of [(*R*)-**1**·**2**]$_n$ in a CHX/THF (95:5 *v/v)* solution. Indeed, the supramolecular dimerization of one of these single rectangular units through van der Waals interactions, dictated most probably by multiple interdigitation of the solubilizing alkyl chains, would lead to the formation of a flat ribbon nanostructure with dimension comparable with the one reported by the SAXS results (4 nm of height and 8 nm of width, Fig. 9c, model (i)). The consequent twisting and dimerization (Fig. 9c, (ii) and (iii) steps, respectively) of the resulting ribbon would allow the formation of the supercoiled fibrous structure observed at the microscale by both TEM and AFM analysis.

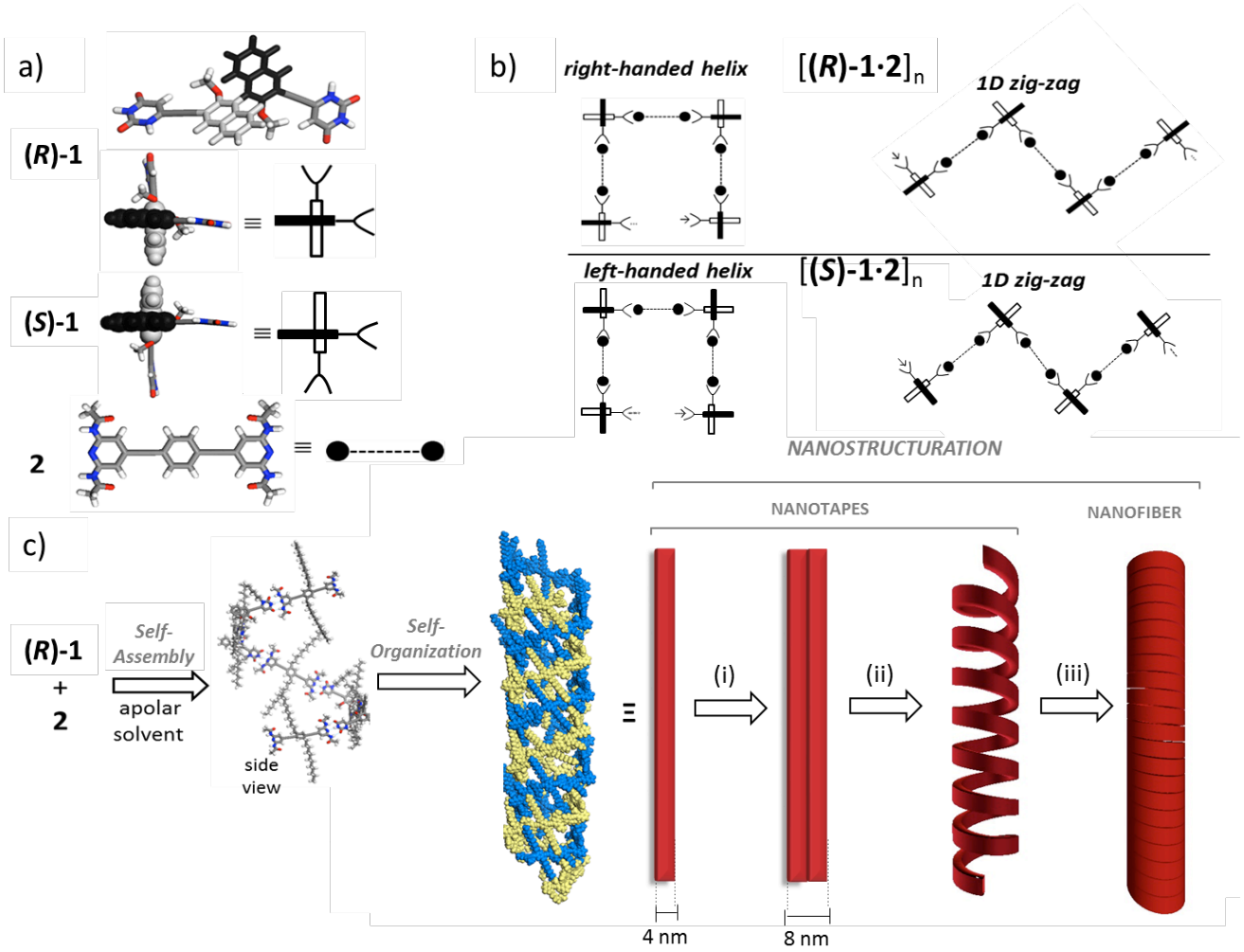

Figure 9. Molecular modeling of the supramolecular polymers of [(*R*)-**1**·**2**]$_n$ and [(*S*)-**1**·**2**]$_n$. a) Side and top views of conformers of (*X*)-**1** along with their sketch representation (on the right). (b) Sketch of the different possible assemblies considered for the molecular mechanics (MM) simulations. (c) Proposed simulated model for self-organized nanofibers (CPK view, one helix in blue, the other in yellow ≃15 nm-long fiber as obtained through several MM simulations cycles of the superstructure): at first, the self-assembly occurs through *H*-bonding between the complementary modules in a helix-type arrangement, which is right- and left-handed for [(*R*)-**1**·**2**]$_n$ and [(*S*)-**1**·**2**]$_n$, respectively, followed by a self-interdigitation of the single helices yielding double helix nanofibers. As observed by SAXS analysis in solution and AFM images on surfaces, it is envisaged that the individual nanofibers are organized into the final superhelical nanofibers by a possible three step mechanism based on the formation of a tape structure (i) that will eventually twist into a single helical tape (ii) and finally dimerize into the final nanofibers structure (iii) observed by TEM and AFM.

From nanospheres to helices. To shed further light on the role of the solvent mixture giving the chiral morphologies, we investigated various solvent mixtures between CHX and THF. As in previous cases, an equimolar amount of molecular modules (*R*)-**1** or (*S*)-**1** and **2** were first dissolved into a minor volume of THF (solvent able to completely solubilize both compounds) and then diluted to the necessary volume with CHX. Aiming at favoring the formation of the most thermodynamically stable architectures, the resulting mixtures were heated and finally drop-casted onto mica surfaces for microscopic analysis and let to evaporate at room temperature. With the more polar mixture (CHX/THF 80:20 *v/v*), the formation of round shaped nanostructures was observed by TEM and TM-AFM investigations (Fig. 10a and 10d). Through detailed TM-AFM analysis, spherical nanoparticles characterized by heights from 10 to 70 nm and thickness of nm to few tens of nm were obtained (Fig. 10a). Interestingly, when a solution of [**1**·**2**]$_n$ was transferred from a CHX/THF (90:10 *v/v*) solution to the mica surface, globular aggregates were predominantly observed, but fibrous material also started to appear (Fig. 10b and 10e). Specifically, the deposited material is characterized by the presence of spherical morphologies that peripherally exposes fibrous ramifications, with diameters between 5 and 50 nm and length up to several μm. With respect to the fibrous morphologies obtained from the CHX/THF (95:5 *v/v*) solutions, the ramifications displayed some substantial structural differences, as they appear as bamboo-like structures. In both cases, SAXS measurements did not reveal any periodicity or formation of homogenous structures. Whereas in the more polar solvent mixture (CHX/THF 80:20 *v/v*) the aggregation seems to be essentially governed by the concentration-driven solutal instability, increasing the apolar character of

the solvent enhances the degree of polymerization, thus favoring the formation of long supramolecular polymers as the solvent evaporates, thus the formation of long fibers.

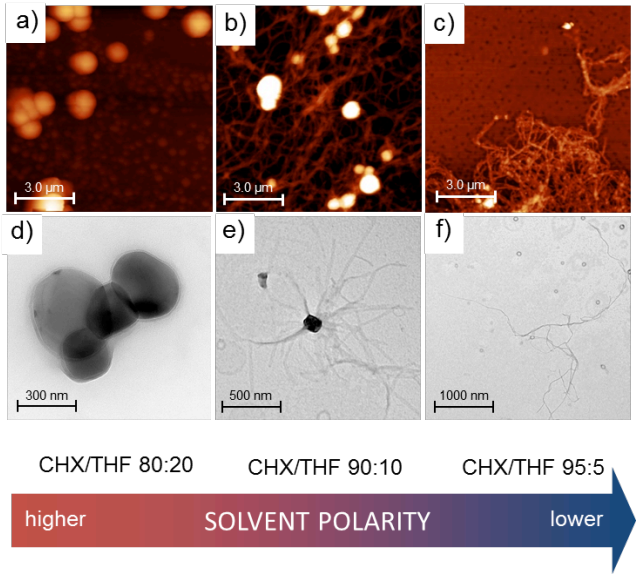

Figure 10. Nanostructuration of the supramolecular polymers into organic morphologies depending on the polarity of the drop-casted solution: (a,d) TM-AFM and TEM images for CHX/THF (80:20 *v/v*); (b,e) images for CHX/THF (90:10 *v/v*) and (c,f) images for CHX/THF (95:5 *v/v*).

Conclusions

We have presented the synthesis and characterization of novel molecular modules carrying hetero-complementary H-bonding recognition motifs. The building block is composed of a BINOL unit which, through its atropoisomers (*R*) and (*S*), served as a chiral unit. Together with a complementary H-bond partner, an achiral linear OPE chromophore, the modules underwent self-assembly through triple H-bonding interactions. The association strength of the triply bonded structures was determined in $CDCl_3$, $CDCl_3$/CHX-d_{12} and Tol-d_8, together with the binding stoichiometry. Through a simple experimental model, we have shown that, together with the association strength, the vapor tension of a given solvent governs the degree of polymerization under evaporation conditions. In particular, solvents favoring strong H-bonded complexes and displaying high vapor pressures induce the formation of high degree of polymerization. Owing to the chromophore unit, it was possible to follow the self-assembly through UV-Vis, CD and fluorescence spectroscopy. Notably, through temperature- and concentration-dependent CD spectroscopy, an isodesmic polymerization mechanism was uncovered. The self-assembled supramolecular polymer has been transferred onto surface for microscopic investigations through AFM and TEM microscopy measurements. Nanostructuration afforded nanorods (from $CHCl_3$), nanofibers ($CHCl_3$/CHX), nanospheres (Tol, CHX/THF 80:20 *v/v*), hybrid nano-sphere/fibers (CHX/THF 90:10 *v/v*) and finally helical nanofibers (CHX/THF 95:5 *v/v*). The self-organization and the chiral transfer from solution to surface were also studied with the aid of SAXS analysis and molecular modeling in order to gain insight into the nanostructuration mechanisms of the material into superhelical nanofibers. These results suggest that if high degrees of polymerization are achieved, fibrous structures apparently expressing chiral morphologies at the microscale can be obtained. The solvophilic character of a given solvent mixture disfavors aggregation phenomena, thus reducing solutal instability. Taken in concert, our experiments showed that the choice of solvent is crucial to dictate the polymorphism of the nanomaterial and the transmission of molecular chirality at higher scales. In particular, an optimal balance between high degree of association, solvent vapor pressure and the solvophobic/solvophilic properties needs to be accomplished in order to control the formation of organic morphologies.

ASSOCIATED CONTENT

Supporting Information

Synthetic protocols and spectroscopic characterisations, titration experiments. This material is available free of charge via the Internet at http://pubs.acs.org.

AUTHOR INFORMATION

Corresponding Authors

davide.bonifazi@unamur.be

mathieu.surin@umons.ac.be

Author Contributions

‡These authors contributed equally.

Notes

The authors declare no competing financial interest.

ACKNOWLEDGMENTS

DB gratefully acknowledges the EU through the ERC Starting Grant "COLORLANDS", the FRS-FNRS (FRFC contracts n° 2.4.550.09), the "TINTIN" ARC project (09/14-023), the MIUR through the FIRB Futuro in Ricerca "SUPRACARBON" (contract n° RBFR10DAK6). NA thanks MIUR (PRIN 2010 INFOCHEM - contract n°. CX2TLM), and Consiglio Nazionale delle Ricerche (Progetto Bandiera N-CHEM). LD and TM thank the University of Trieste for their doctoral fellowships. J.R.-M. is a FNRS post-doctoral researcher and M.S. is a FNRS research associate. The collaboration between Mons and Namur is supported by the FNRS through the FRFC-BINDER project (grant n° 2.4615.11) and the Belgian Government (IAP-PAI P7 network "Functional Supramolecular Systems"). Mr. C. Gamboz is acknowledged for the help with the TEM imaging.

REFERENCES

(1) (a) Lehn, J. M., *Science* **2002,** *295*, 2400-2403; (b) Lehn, J. M., *Proc. Natl. Acad. Sci. U.S.A.* **2002,** *99*, 4763-4768; (c) Whitesides, G. M.; Grzybowski, B., *Science* **2002,** *295*, 2418-2421.

(2) (a) Aida, T.; Meijer, E. W.; Stupp, S. I., *Science* **2012,** *335*, 813-817; (b) Busseron, E.; Ruff, Y.; Moulin, E.; Giuseppone, N., *Nanoscale* **2013,** *5*, 7098-7140; (c) Santhosh Babu, S.; Praveen, V. K.; Ajayaghosh, A., *Chem. Rev.* **2014,** *114*, 1973-2129; (d) Stupp, S. I.; Palmer, L. C., *Chem. Mater.* **2014,** *26*, 507-518; (e) Dong, R.; Zhou, Y.; Huang, X.; Zhu, X.; Lu, Y.; Shen, J., *Adv. Mater.* **2015,** *27*, 498-526.

(3) (a) Santhosh Babu, S.; Prasanthkumar, S.; Ajayaghosh, A., *Angew. Chem. Int. Ed.* **2012,** *51*, 1766-1776; (b) Ceroni, P.; Credi, A.; Venturi, M., *Chem. Soc. Rev.* **2014,** *43*, 4068; (c) Praveen, V. K.; Ranjith, C.; Bandini, E.; Ajayaghosh, A.; Armaroli, N., *Chem. Soc. Rev.* **2014,** *43*, 4222-4242; (d) Xu, J.; Semin, S.; Rasing, T.; Rowan, A. E., *Small* **2014,** *11*, 1113-1129; (e) Yan, Q.; Luo, Z.; Cai, K.; Ma, Y.; Zhao, D., *Chem. Soc. Rev.* **2014,** *43*, 4199-4221.

(4) (a) Bunz, U. H. F., *Chem. Rev.* **2000,** *100*, 1605-1644; (b) Ajayaghosh, A.; Varghese, R.; Praveen, V. K.; Mahesh, S., *Angew. Chem. Int. Ed.* **2006,** *45*, 3261-3264; (c) Garcia, F.; Sanchez, L., *J. Am. Chem. Soc.* **2012,** *134*, 734-742; (d) Ajayaghosh, A.; Varghese, R.; Mahesh, S.; Praveen, V. K., *Angew. Chem. Int. Ed.* **2006,** *45*, 7729-7732.

(5) (a) Ajayaghosh, A.; Praveen, V. K., *Acc. Chem. Res* **2007,** *40*, 644-656; (b) Schenning, A. P.; Meijer, E. W., *Chem. Commun.* **2005**, 3245-3258; (c) Moulin, E.; Cid, J. J.; Giuseppone, N., *Adv. Mater.* **2013,** *25*, 477-487.

(6) (a) Hill, J. P.; Jin, W.; Kosaka, A.; Fukushima, T.; Ichihara, H.; Shimomura, T.; Ito, K.; Hashizume, T.; Ishii, N.; Aida, T., *Science* **2004,** *304*, 1481-1483; (b) Wu, J.; Pisula, W.; Müllen, K., *Chem. Rev.* **2007,** *107*, 718-747; (c) Ito, S.; Herwig, P. T.; Böhme, T.; Rabe, J. P.; Rettig, W.; Müllen, K., *J. Am. Chem. Soc.* **2000,** *122*, 7698-7706; (d) Dossel, L. F.; Kamm, V.; Howard, I. A.; Laquai, F.; Pisula, W.; Feng, X.; Li, C.; Takase, M.; Kudernac, T.; De Feyter, S.; Müllen, K., *J. Am. Chem. Soc.* **2012,** *134*, 5876-5886; (e) Seyler, H.; Purushothaman, B.; Jones, D. J.; Holmes, A. B.; Wong, W. W. H., *Pure Appl. Chem.* **2012,** *84*, 1047–1067.

(7) (a) Elacqua, E.; Lye, D. S.; Weck, M., *Acc. Chem. Res* **2014,** *47*, 2405-16; (b) Jonkheijm, P.; Hoeben, F. J. M.; Kleppinger, R.; van Herrikhuyzen, J.; Schenning, A. P. H. J.; Meijer, E. W., *J. Am. Chem. Soc.* **2003,** *125*, 15941-15949; (c) Puigmartí-Luis, J.; Minoia, A.; Pérez del Pino, Á.; Ujaque, G.; Rovira, C.; Lledos, A.; Lazzaroni, R.; Amabilino, D. B., *Chem. Eur. J.* **2006,** *12*, 9161-9175; (d) Chithra, P.; Varghese, R.; Divya, K. P.; Ajayaghosh, A., *Chem. Asian J.* **2008,** *3*, 1365-1373; (e) Puigmartí-Luis, J.; Pérez del Pino, Á.; Laukhina, E.; Esquena, J.; Laukhin, V.; Rovira, C.; Vidal-Gancedo, J.; Kanaras, A. G.; Nichols, R. J.; Brust, M.; Amabilino, D. B., *Angew. Chem. Int. Ed.* **2008,** *47*, 1861-1865; (f) Yagai, S.; Aonuma, H.; Kikkawa, Y.; Kubota, S.; Karatsu, T.; Kitamura, A.; Mahesh, S.; Ajayaghosh, A., *Chem. Eur. J.* **2010,** *16*, 8652-8661; (g) Gopal, A.; Varghese, R.; Ajayaghosh, A., *Chem. Asian J.* **2012,** *7*, 2061-2067.

(8) (a) Pirondini, L.; Stendardo, A. G.; Geremia, S.; Campagnolo, M.; Samorì, P.; Rabe, J. P.; Fokkens, R.; Dalcanale, E., *Angew. Chem. Int. Ed.* **2003,** *42*, 1384-1387; (b) Surin, M.; Samorì, P.; Jouaiti, A.; Kyritsakas, N.; Hosseini, M. W., *Angew. Chem. Int. Ed.* **2007,** *46*, 245-249; (c) Northrop, B. H.; Yang, H. B.; Stang, P. J., *Chem. Commun.* **2008,** *45*, 5896-5908; (d) Imaz, I.; Rubio-Martinez, M.; Saletra, W. J.; Amabilino, D. B.; Maspoch, D., *J. Am. Chem. Soc.* **2009,** *131*, 18222-18223; (e) Northrop, B. H.; Zheng, Y. R.; Chi, K. W.; Stang, P. J., *Acc. Chem. Res* **2009,** *42*, 1554-1563; (f) Ciesielski, A.; Piot, L.; Samorì, P.; Jouaiti, A.; Hosseini, M. W., *Adv. Mater.* **2009,** *21*, 1131-1136; (g) El Garah, M.; Ciesielski, A.; Marets, N.; Bulach, V.; Hosseini, M. W.; Samori, P., *Chem. Commun.* **2014,** *50*, 12250-12253; (h) Caricato, M.; Delforge, A.; Bonifazi, D.; Dondi, D.; Mazzanti, A.; Pasini, D., *Org Biomol Chem* **2015,** *13*, 3593-601.

(9) Lehn, J.-M., *Angew. Chem. Int. Ed.* **1988,** *27*, 89-112.

(10) (a) Brunsveld, L.; Vekemans, J. A. J. M.; Hirschberg, J. H. K. K.; Sijbesma, R. P.; Meijer, E. W., *Proc. Natl. Acad. Sci. U.S.A.* **2002,** *99*, 4977-4982; (b) Amabilino, D. B.; Stoddart, J. F.; Williams, D. J., *Chem. Mater.* **1994,** *6*, 1159-1167; (c) Bowden, N., *Science* **1997,** *276*, 233-235; (d) Orr, G. W., *Science* **1999,** *285*, 1049-1052; (e) Pérez-García, L.; Amabilino, D. B., *Chem. Soc. Rev.* **2002,** *31*, 342-356; (f) Pérez-García, L.; Amabilino, D. B., *Chem. Soc. Rev.* **2007,** *36*, 941-967; (g) Gomar-Nadal, E.; Puigmartí-Luis, J.; Amabilino, D. B., *Chem. Soc. Rev.* **2008,** *37*, 490-504; (h) Yagai, S.; Yamauchi, M.; Kobayashi, A.; Karatsu, T.; Kitamura, A.; Ohba, T.; Kikkawa, Y., *J. Am. Chem. Soc.* **2012,** *134*, 18205-18208; (i) Pfukwa, R.; Kouwer, P. H. J.; Rowan, A. E.; Klumperman, B., *Angew. Chem. Int. Ed.* **2013,** *52*, 11040-11044.

(11) (a) Li, M.; Xu, S.; Kumacheva, E., *Macromolecules* **2000,** *33*, 4972-4978; (b) Carvalho, A. J.; Pereira-da-Silva, M. A.; Faria, R. M., *Eur. Phys. J. E* **2006,** *20*, 309-315; (c) Thiele, U.; Vancea, I.; Archer, A. J.; Robbins, M. J.; Frastia, L.; Stannard, A.; Pauliac-Vaujour, E.; Martin, C. P.; Blunt, M. O.; Moriarty, P. J., *J. Phys. Condens. Matter* **2009,** *21*, 264016; (d) Li, B.; Puigmartí-Luis, J.; Jonas, A. M.; Amabilino, D. B.; De Feyter, S., *Chem. Commun.* **2014,** *50*, 13216-13219.

(12) (a) Voorhees, P. W., *J. Stat. Phys.* **1985,** *38*, 231-252; (b) Mahesh, S.; Gopal, A.; Thirumalai, R.; Ajayaghosh, A., *J. Am. Chem. Soc.* **2012,** *134*, 7227-30.

(13) (a) Reiter, G., *Phys. Rev. Lett.* **1992,** *68*, 75-78; (b) Maeda, H., *Langmuir* **2000,** *16*, 9977-9982; (c) Gonuguntla, M.; Sharma, A., *Langmuir* **2004,** *20*, 3456-3463.

(14) (a) Karthaus, O.; Gråsjö, L.; Maruyama, N.; Shimomura, M., *Thin Solid Films* **1998,** *327-329*, 829-832; (b) Weh, L., *J. Colloid Interface Sci.* **2001,** *235*, 210-217.

(15) (a) van Dijk, M. A.; van den Berg, R., *Macromolecules* **1995,** *28*, 6773-6778; (b) Kim, G.; Libera, M., *Macromolecules* **1998,** *31*, 2569-2577.

(16) Marangoni, T.; Mezzasalma, S. A.; Llanes-Pallas, A.; Yoosaf, K.; Armaroli, N.; Bonifazi, D., *Langmuir* **2011,** *27*, 1513-1523.

(17) (a) Terfort, A.; Bowden, N.; Whitesides, G. M., *Nature* **1997,** *386*, 162-164; (b) Puigmartí-Luis, J.; Pérez del Pino, Á.; Laukhin, V.; Feldborg, L. N.; Rovira, C.; Laukhina, E.; Amabilino, D. B., *J. Mater. Chem.* **2010,** *20*, 466; (c) Gillissen, M. A. J.; Koenigs, M. M. E.; Spiering, J. J. H.; Vekemans, J. A. J. M.; Palmans, A. R. A.; Voets, I. K.; Meijer, E. W., *J. Am. Chem. Soc.* **2014,** *136*, 336-343; (d) Hollamby, M. J.; Karny, M.; Bomans, P. H. H.; Sommerdijk, N. A. J. M.; Saeki, A.; Seki, S.; Minamikawa, H.; Grillo, I.; Pauw, B. R.; Brown, P.; Eastoe, J.; Möhwald, H.; Nakanishi, T., *Nat. Chem.* **2014,** *6*, 690-696.

(18) (a) Amabilino, D. B.; Veciana, J., *Top. Curr. Chem.* **2006,** *265*, 253-302; (b) Palmans, A. R. A.; Meijer, E. W., *Angew. Chem. Int. Ed.* **2007,** *46*, 8948-8968; (c) Crassous, J., *Chem. Soc. Rev.* **2009,** *38*, 830-845; (d) Amabilino, D. B., *Chem. Soc. Rev.* **2009,** *38*, 669-670; (e) Coquerel, G.; Amabilino, D. B., The Nanoscale Aspects of Chirality in Crystal Growth: Structure and Heterogeneous Equilibria. In *Chirality at the Nanoscale: Nanoparticles, Surfaces, Materials and more*, Amabilino, D. B., Ed. Wiley: Weinheim, 2009; pp 305-348; (f) Zhang, L.; Qin, L.; Wang, X.; Cao, H.; Liu, M., *Adv. Mater.* **2014,** *26*, 6959-6964.

(19) (a) Mohnani, S.; Llanes-Pallas, A.; Bonifazi, D., *Pure Appl. Chem.* **2010,** *82*, 917–929; (b) Yoosaf, K.; Llanes-Pallas, A.; Marangoni, T.; Belbakra, A.; Marega, R.; Botek, E.; Champagne, B.; Bonifazi, D.; Armaroli, N., *Chem. Eur. J.* **2011,** *17*, 3262-3273.

(20) (a) Bonifazi, D.; Mohnani, S.; Llanes-Pallas, A., *Chem. Eur. J.* **2009,** *15*, 7004-7025; (b) Marangoni, T.; Bonifazi, D., *Nanoscale* **2013,** *5*, 8837-8851.

(21) Yoosaf, K.; Belbakra, A.; Armaroli, N.; Llanes-Pallas, A.; Bonifazi, D., *Chem. Commun.* **2009**, 2830-2832.

(22) (a) Piot, L.; Palma, C.-A.; Llanes-Pallas, A.; Prato, M.; Szekrényes, Z.; Kamarás, K.; Bonifazi, D.; Samorì, P., *Adv. Funct. Mater.* **2009,** *19*, 1207-1214; (b) Llanes-Pallas, A.; Palma, C. A.; Piot, L.; Belbakra, A.; Listorti, A.; Prato, M.; Samorì, P.; Armaroli, N.; Bonifazi, D., *J. Am. Chem. Soc.* **2009,** *131*, 509-520.

(23) Llanes-Pallas, A.; Matena, M.; Jung, T.; Prato, M.; Stohr, M.; Bonifazi, D., *Angew. Chem. Int. Ed.* **2008,** *47*, 7726-7730.

(24) (a) Brunel, J. M., *Chem. Rev.* **2005,** *105*, 857-898; (b) Caricato, M.; Sharma, A. K.; Coluccini, C.; Pasini, D., *Nanoscale* **2014,** *6*, 7165-7174; (c) Hill, D. J.; Moore, J. S., *Proc. Natl. Acad. Sci. U.S.A.* **2002,** *99*, 5053-5057.

(25) Hua, J.; Lin, W., *Org. Lett.* **2004,** *6*, 861-864.

(26) Cook, J. L.; Hunter, C. A.; Low, C. M.; Perez-Velasco, A.; Vinter, J. G., *Angew. Chem. Int. Ed.* **2007,** *46*, 3706-3709.

(27) Beijer, F. H.; Sijbesma, R. P.; Vekemans, J. A. J. M.; Meijer, E. W.; Kooijman, H.; Spek, A. L., *J. Org. Chem.* **1996,** *61*, 6371-6380.

(28) (a) Ciferri, A., *Macromol. Rapid Commun.* **2002,** *23*, 511-529; (b) Michelsen, U.; Hunter, C. A., *Angew. Chem. Int. Ed.* **2000,** *39*, 764-767.

(29) (a) Macchioni, A.; Ciancaleoni, G.; Zuccaccia, C.; Zuccaccia, D., *Chem. Soc. Rev.* **2008,** *37*, 479-489; (b) Avram, L.; Cohen, Y., *Chem. Soc. Rev.* **2014,** *44*, 586-602; (c) Cohen, Y.; Avram, L.; Frish, L., *Angew. Chem. Int. Ed.* **2005,** *44*, 520-554.

(30) (a) Li, B.; Puigmartí-Luis, J.; Jonas, A. M.; Amabilino, D. B.; De Feyter, S., *Chem. Commun.* **2014,** *50*, 13216-13219; (b) Grosso, D.; Cagnol, F.; Soler-Illia, G. J. d. A. A.; Crepaldi, E. L.; Amenitsch, H.; Brunet-Bruneau, A.; Bourgeois, A.; Sanchez, C., *Adv. Funct. Mater.* **2004,** *14*, 309-322; (c) Brinker, C. J.; Lu, Y.; Sellinger, A.; Fan, H., *Adv. Mater.* **1999,** *11*, 579-585.

(31) (a) Sijbesma, R. P., *Science* **1997,** *278*, 1601-1604; (b) Brunsveld, L.; Folmer, B. J. B.; Meijer, E. W.; Sijbesma, R. P., *Chem. Rev.* **2001,** *101*, 4071-4098; (c) De Greef, T. F.; Smulders, M. M.; Wolffs, M.; Schenning, A. P.; Sijbesma, R. P.; Meijer, E. W., *Chem. Rev.* **2009,** *109*, 5687-5754.

(32) While the solubility of compound **2** in toluene is low, it becomes more soluble once that **1** equivalent of compound 1 is added.

(33) Surin, M.; Janssen, P. G. A.; Lazzaroni, R.; Leclère, P.; Meijer, E. W.; Schenning, A. P. H. J., *Adv. Mater.* **2009,** *21*, 1126-1130.

(34) (a) Spano, F. C., *Acc. Chem. Res* **2010,** *43*, 429-439; (b) Zhao, Y. S.; Fu, H.; Peng, A.; Ma, Y.; Xiao, D.; Yao, J., *Adv. Mater.* **2008,** *20*, 2859-2876.

(35) (a) Roe, R. J., *Methods of X-ray and neutron scattering in polymer science*. Oxford University Press: New York, 2000; (b) Patterson, J. P.; Robin, M. P.; Chassenieux, C.; Colombani, O.; O'Reilly, R. K., *Chem. Soc. Rev.* **2014,** *43*, 2412; (c) Otto Glatter, O. K., *Small Angle X-ray Scattering*. Academic Press: London, 1982.

(36) Teixeira, C. V.; Amenitsch, H.; Fukushima, T.; Hill, J. P.; Jin, W.; Aida, T.; Hotokka, M.; Linden, M., *J. Appl. Cryst.* **2010,** *43*, 850-857.

(37) In order to elucidate the geometric organization of the self-assembled molecular models along the twisted ribbon system, more complex fitting models taking into account also its possible internal structure were also used. However, the results were not statistically significant, and thus they were not considered.

(38) (a) Sun, H., *J. Phys. Chem. B* **1998,** *102*, 7338-7364; (b) Ren, Z.; Zeng, X.; Yang, X.; Ma, D.; Hsu, S. L., *Polymer* **2005,** *46*, 12337-12347; (c) Ziegler, A.; Mamdouh, W.; Ver Heyen, A.; Surin, M.; Uji-i, H.; Abdel-Mottaleb, M. M. S.; De Schryver, F. C.; De Feyter, S.; Lazzaroni, R.; Höger, S., *Chem. Mater.* **2005,** *17*, 5670-5683; (d) Lei, S.; Ver Heyen, A.; De Feyter, S.; Surin, M.; Lazzaroni, R.; Rosenfeldt, S.; Ballauff, M.; Lindner, P.; Mossinger, D.; Höger, S., *Chem. Eur. J.* **2009,** *15*, 2518-35.

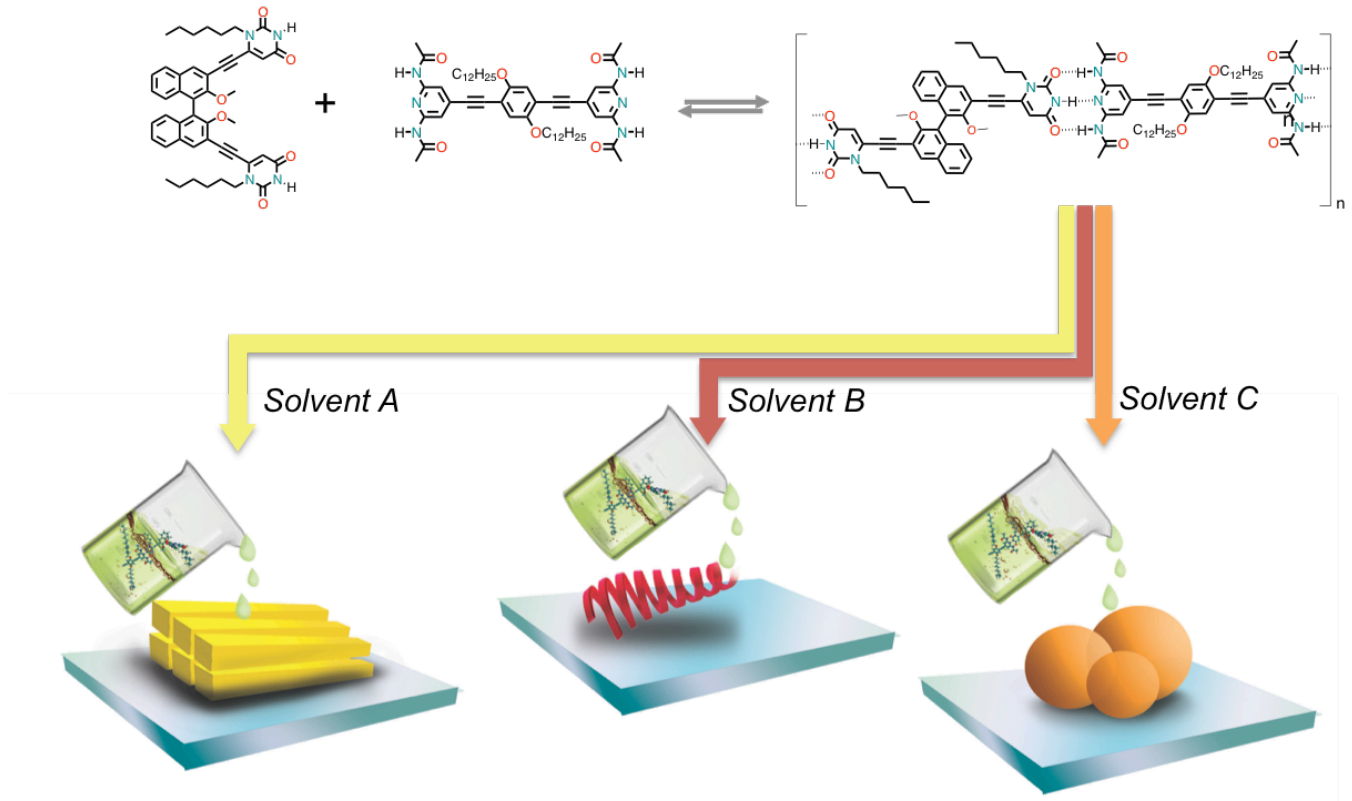
Solvent A
Solvent B
Solvent C